

Morphology and Kinetic Study of the Interfacial Reaction between the Sn-3.5Ag Solder and Electroless Ni-P Metallization

ZHONG CHEN,^{1,3} MIN HE,¹ and GUOJUN Qi²

1.—School of Materials Engineering, Nanyang Technological University, Singapore 639798. 2.—Singapore Institute of Manufacturing Technology, Singapore 638075. 3.—E-mail: aszchen@ntu.edu.sg

This work summarizes the interfacial reaction between lead-free solder Sn-3.5Ag and electrolessly plated Ni-P metallization in terms of morphology and growth kinetics of the intermetallic compounds (IMC). Comparison with pure Ni metallization is made in order to clarify the role of P in the solder reaction. During reflow, the IMCs formed with the Ni-P under-bump metallization (UBM) exist in chunky crystal blocks and small crystal agglomerates, while the ones with the sputtered Ni UBM exhibit uniformly scallop grains with faceted surfaces. The IMC thickness increases with reflow time following approximately a $t^{1/3}$ power law for both systems. The IMC growth rate is higher with the Ni-P UBM than the Ni UBM. The thickness of the Ni₃Sn₄ layer increases linearly with the square root of thermal aging time, indicating that the growth of the IMCs is a diffusion-controlled process. The activation energy for Ni₃Sn₄ growth in solid-state reaction is found to be 110 kJ/mol and 91 kJ/mol for the Ni-P and sputtered Ni UBMs, respectively. Kirkendall voids are detected inside the Ni₃P layer in the Sn-3.5Ag/Ni-P system. No such voids are found in the Sn-3.5Ag/Ni system.

Key words: Lead-free solder, electroless Ni-P, intermetallic compound (IMC), under-bump metallization (UBM)

INTRODUCTION

The coming “green” era anticipates wider application of Pb-free solders in the semiconductor industry. So far, intensive research has been carried out on lead-free solders, which enables the semiconductor industry to narrow down their choices to the two most promising systems: Sn-Ag or Sn-Ag-Cu. One common feature of the two systems is that both contain a high percentage of Sn. Typical reliability issues with these high Sn content, high (compared to eutectic Sn-Pb) melting-temperature solders is the rapid consumption of the main element Cu in the conventional under-bump metallization (UBM), leading to spallation of Cu-Sn intermetallic compounds (IMCs).^{1–4} To answer the challenge, Ni-based UBMs, such as electroless Ni or sputtered Ni, have been proposed as alternatives. They have been reported to have slower reaction with Sn-containing solders than the Cu-

based UBM.² Among them, electrolessly plated Ni has the advantage of not only good solderability but also plating selectivity and low process cost.^{5,6}

Complications arise with the application of electroless Ni as the UBM because of the fact that electroless Ni is actually an amorphous alloy of Ni with 6–13wt.%P. The inevitable introduction of P during plating complicates the solder reaction at the interface. As a result, many studies have been focused on the interaction between electroless Ni (referred to as Ni-P hereafter) and Sn-based solders.^{7–24} Yet, there are still many outstanding issues that need to be further investigated. A number of experiments have observed the crystallization of the amorphous Ni-P triggered by the formation of the Ni₃Sn₄ IMC. The crystallization leads to the formation of an additional P-rich layer in between the Ni₃Sn₄ IMC layer and the Ni-P UBM.^{10–12,17–22} However, more work is needed to understand the phase transformation in this layer. Some reported the layer to consist of the Ni₃P phase^{1,10,17} but others a mixture of Ni₃P and

(Received March 12, 2004; accepted June 25, 2004)

Ni.^{5,20} Under extended annealing conditions, mixed layers of Ni₃P and Ni₁₂P₅ were reported.⁵ Alam et al.²⁴ reported that, when reflowing Sn-containing solders on a high P content (20 at.%) Ni-P UBM, Ni₃P is the only compound initially present. During prolonged reflow, new phases of Ni₂P, Ni₅P₄, and NiP₂ are also formed. Leaving these fine details aside for the time being, all the evidence shows that the crystallization of the Ni-P UBM leads to the formation of a layer dominated by Ni₃P.¹⁹

In addition to the Ni₃P-dominated layer (referred to as the Ni₃P layer thereafter), there exists a third layer in between the Ni₃Sn₄ and Ni₃P layers, which consists of Ni, Sn, and P.^{1,19–22} This layer has been identified either as Ni-Sn-P without fixed stoichiometric details,^{1,19} Ni₂SnP,²² or Ni₃SnP.²⁰ Again, how this layer/phase has been formed needs to be studied carefully.

Despite all these differences, what can be concluded at this moment is that these layers are clearly byproducts caused by the introduction of P in the UBM. In other words, if there were no P in the UBM, the Ni₃P and ternary Ni-Sn-P layers would not have formed in the soldering reaction.

Observation of voids at the interface also seems to be uniquely related to the use of the Ni-P UBM. Zeng and Tu¹ reported Kirkendall voids in SnAgCu solder/Ni-P UBM samples reflowed for five times. Jeon et al.¹⁷ used transmission electron microscopy (TEM) to study the reaction of the Ni-P UBM with both Sn-Pb and Sn-Ag solders in liquid-state reaction. They reported Kirkendall voids inside the Ni₃Sn₄ layer at the locations close to the Ni₃P layer. The current authors observed voids in the Ni₃P layer in both eutectic Sn-Pb/Ni-P and Sn-3.5Ag/Ni-P systems.^{18,19} We believe that the presence of the two interfacial layers is the reason for the unbalanced interdiffusion between Sn in the solder and Ni in the UBM, leading to the formation of Kirkendall voids.^{18,19} This view will be elaborated further in this paper. In summary, various findings and explanations have been reported on the interfacial reaction between different types of solder with the Ni-P UBM. Discrepancy exists among these observations and their corresponding explanations.

In this paper, we report the experimental results of the solder reaction between the Sn-3.5Ag solder and two types of Ni-based UBMs: electroless Ni-P and sputtered pure Ni. The growth kinetics of the Ni-Sn IMC and the effect of reflow and aging treatment on the morphology of IMCs are examined. By comparing these two UBMs with the same Pb-free solder, the role of P in the interfacial reaction is highlighted. The formation mechanism of Kirkendall voids with the Ni-P UBM has been discussed. The interfacial reaction between the Sn-3.5Ag solder and the two UBMs will be summarized.

EXPERIMENTAL PROCEDURES

The substrates used in this study were prepared from blank Si wafers. A 0.1- μm -thick Cr layer was

sputtered first, followed by sputter deposition of about 1- μm Ni and 0.3- μm Au. The Cr layer provides good adhesion of the UBM to the wafer, and the Au layer is to protect the Ni surface from oxidation. The sputtered Au/Ni stack was used as a reference UBM to compare with the Ni-P UBM. The sputtered Ni was also used as the seed layer for the subsequent electroless nickel plating. The Ni-P (containing 12.5at.%P) UBM of about 5 μm was obtained by electroless plating with a commercial solution on the preceding sputtered Ni substrate. Before the plating, the sputtered 0.3- μm Au layer was etched away. A final finish of immersion gold of ~ 0.03 - μm thick on the plated Ni-P was applied as a surface protection.

The Sn-3.5Ag solder was in the form of wire with no-clean reflow flux in the core. Samples with both Ni-based UBMs were prepared by reflow at 251°C for holding times ranging from 5 sec to 5 h. They were then taken out of the oven and cooled in air. Samples reflowed for 180 sec were thermally aged at 130°C, 150°C, 170°C, and 190°C for various durations in air.

Scanning electron microscopy (SEM) observations were made on the cross section and from the top of the IMCs at the solder/UBM interface. The common metallography practice was used to prepare the samples. An etchant of 2% HCl was used to reveal the cross-sectional microstructure. To observe the top view of the IMCs, the majority of the solder on the specimens were mechanically ground away first. The ground specimens were then soaked in 2% HCl solution to dissolve the remaining solder. The average thickness of the IMC was obtained by measuring the cross-section area of the IMC layer over a certain length from SEM images.

The microstructure of the interfacial reaction was also investigated by cross-sectional TEM. The TEM samples were prepared by diamond saw cutting to a thickness of about 200 μm and then grinding using double-side mechanical dimpling. A thin area of about 20 μm could be achieved in the center by this approach. A cold-stage Ar⁺ ion milling at liquid nitrogen temperature was used to prevent the sample from high temperature damage. The TEM observations were performed using a JEOL JEM 2010 microscope (Japan Electron Optics, Tokyo) operating at 200 kV. A microprobe beam of ~ 0 nm in diameter was used for the composition analysis using energy-dispersive x-ray (EDX) analysis.

RESULTS

Liquid-State Solder: UBM Reaction

IMC Morphology during Liquid-State Reaction

Figure 1 reveals the interfacial microstructures of the Sn-3.5Ag solder with the Ni-P and Ni UBMs, respectively, after reflow at 251°C for 180 sec. A Ni₃P layer is clearly visible between Ni₃Sn₄ and the Ni-P UBM. At relatively short reflow time, the ternary layer Ni-Sn-P is not visible under SEM. With the Ni UBM, only the Ni₃Sn₄ IMC forms between the solder

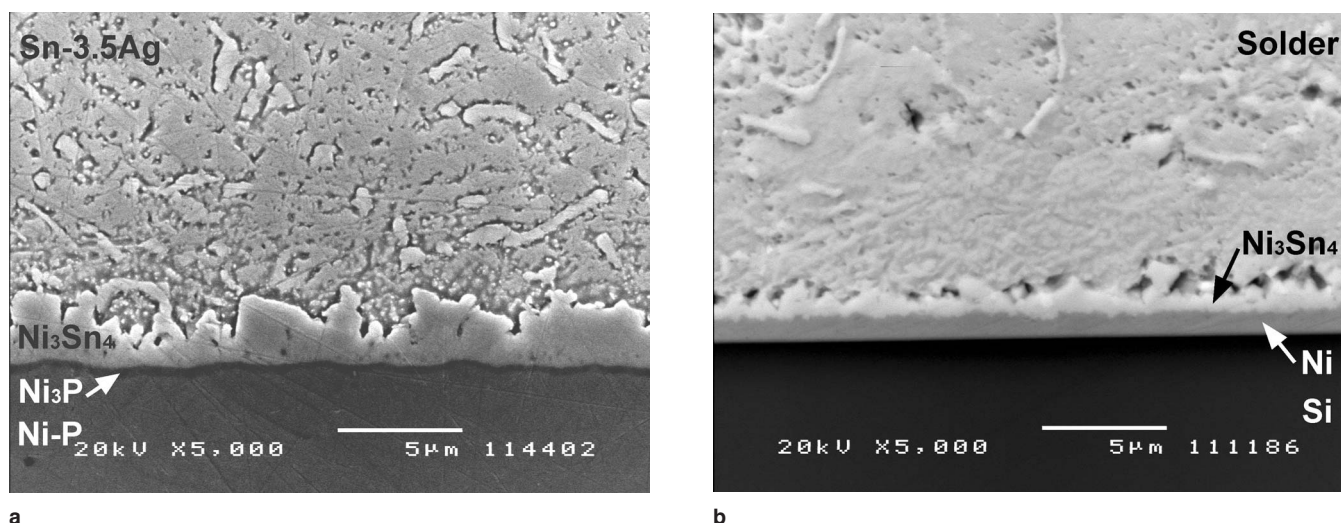


Fig. 1. The Sn-3.5Ag solder with Ni-based UBMs reflowed for 180 sec at 251°C: (a) electroless Ni-P UBM and (b) sputtered Ni UBM. The Ni₃P layer is visible in the Ni-P system.

and unconsumed Ni. The Au dissolves readily into the molten solder soon after reflow begins; no Au IMC was detected at the interface. These observations of the main interfacial reaction products are in agreement with what were reported by other researchers.^{7,10,17,25} Under the same reflow condition, the borderline between Ni₃Sn₄ and the Ni UBM is flatter than the Ni-P UBM (compare Fig. 1a and b). Another clear difference is that the Ni₃Sn₄ IMC layer formed with the sputtered Ni UBM is thinner than that with the Ni-P UBM system under the same reflow condition.

The top views of the IMC reveal a changing morphology on the Ni-P UBM.²⁶ With 30-sec reflow on the Ni-P UBM, the majority of the IMC grains is needle-like IMC. When reflow time extends to 90 sec, the majority of the IMC grains changes to boomerang type and chunk type. Grain sizes of both boomerang- and chunk-type grains increase with reflow time. When reflow time increases to 600 sec, IMC needles

completely disappear; only the faceted chunk-type IMCs remain. The IMCs formed on the Ni UBM, on the other hand, are all scallop-type grains with faceted surfaces. Their size is smaller, and there is no change in shape as in the case of the Ni-P UBM.

IMC Growth during Liquid-State Reaction

After its formation, the IMC grain coarsens and facets continuously in a prolonged reflow process. The facet is due to the anisotropic interfacial energy of the Ni₃Sn₄ phase. To quantify the growth of the Ni₃Sn₄ layer, the relationship between the layer thickness, δ , and the reflow time, t , is curve-fitted into an empirical power law:

$$\delta = k_1 t^{1/n} \quad (1)$$

where k_1 and n are constants, which are obtained by linear fitting the log-log plot from experimental data shown in Fig. 2. The best fit of all experimental data describing the thickening kinetics is listed in Table I.

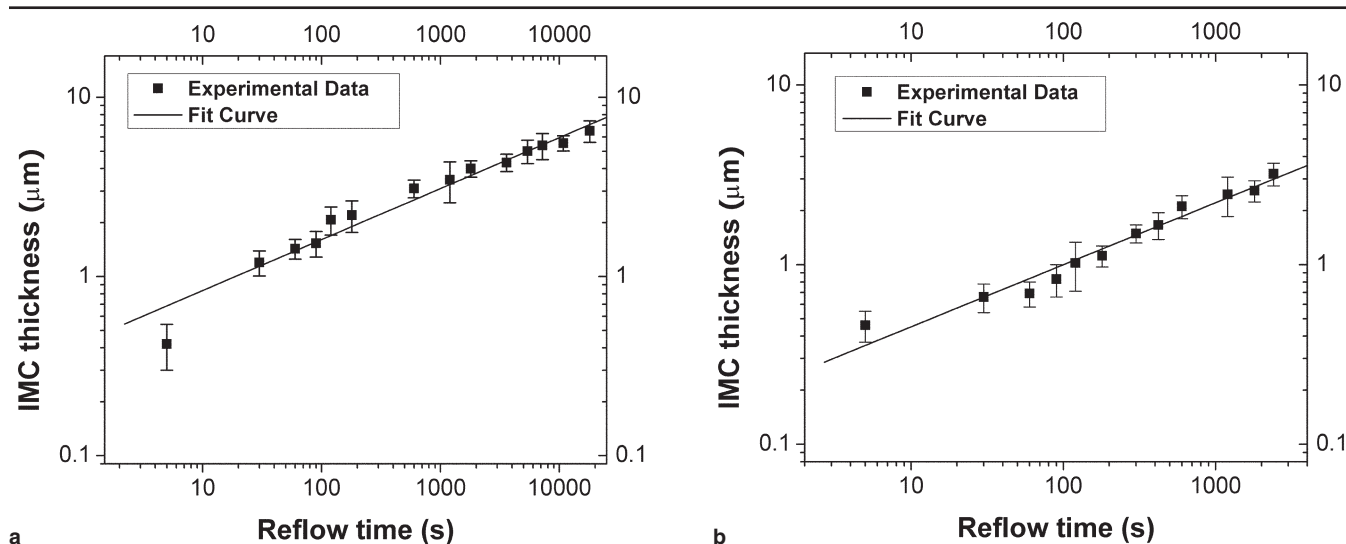


Fig. 2. Log-log plot of Ni₃Sn₄ IMC thickening kinetics during liquid-state reaction: (a) Sn-3.5Ag/Ni-P UBM and (b) Sn-3.5Ag/Ni UBM.

Table I. Kinetics Parameters for the Growth of the Ni_3Sn_4 IMC in Sn-3.5Ag with Ni-P and Ni UBMs during Liquid-State Reaction

UBM	k_1	n	$1/n$
Ni-P alloy	0.43	3.57	0.28
Sputtered Ni	0.20	2.86	0.35

The growth kinetics parameter shows that the IMC thickness has an approximate $t^{1/3}$ dependence on time for both UBMs. In addition, the IMC grows faster with the Ni-P UBM than with the Ni UBM.

When the 1- μm -thick Ni UBM has been consumed after around 40-min reflow, spallation and delamination of Ni_3Sn_4 grains can be observed, as shown in Fig. 3. The delamination indicates that Ni_3Sn_4 does not wet the underlying Cr layer. To verify that complete consumption of Ni is indeed the cause for the delamination, an additional experiment was carried out reflowing the solder on a Ni foil (250 μm , 99.98% purity). In this case, Ni was not fully reacted even after extremely long-time reflow. It was found that some IMCs spalled into the molten solder, but there was always a layer of IMC that adheres to the underlying Ni UBM well. Figure 4 shows such a result after 18-h reflow with the Ni foil.

In the Ni-P UBM system, neither delamination nor spallation of the Ni_3Sn_4 IMC was observed even after reflow for 5 h at 251°C. Because the Ni-P layer is 5- μm thick, it is easy to understand why there is no delamination. Comparing the results with the Ni-P, the thin Ni UBMs, and the Ni foil, current work finds that the wettability/adhesion of the Ni_3Sn_4 IMC on the Ni-based UBM is generally very good; delamination occurs only when the UBM has been completely consumed. Some IMCs still spall into the molten solders when there is a layer of well-adhered IMCs. This type of spallation happens more easily with the Ni UBM than the Ni-P UBM. The reason for this will be discussed later.

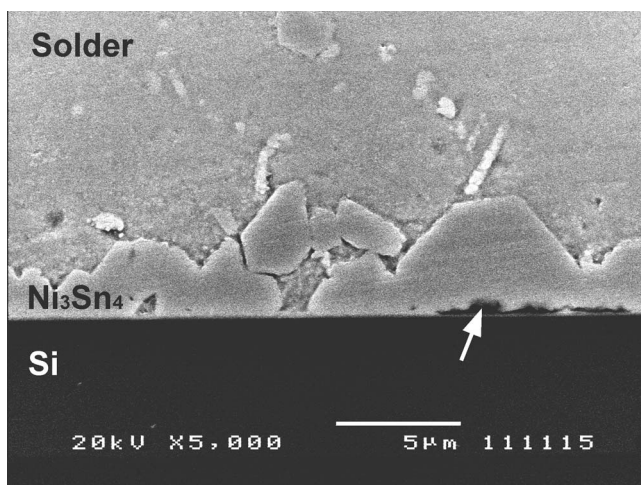


Fig. 3. The IMC spallation and delamination from the substrate after reflowed for 40 min when the sputtered Ni UBM is fully consumed. Arrow indicates the location of delamination.

Kirkendall Void Formation during Liquid-State Reaction

From samples of the Sn-3.5Ag/Ni-P UBM system, voids are easily observable under SEM inside the Ni_3P layer. A typical view of the voids is shown in Fig. 5. Such voids only exist in the samples with the Ni-P UBM after long-time reflow (>30 min), and they grow in size with reflow time. No voids are observed in the Ni system even after reflow at 251°C for 18 h (Fig. 4).

The Phase Composition of the Ni_3P and Ni-Sn-P Layers

It was clearly shown that beside the Ni_3Sn_4 layer, two more layers exist at the Sn-3.5Ag/Ni-P interface.¹⁹ In the current work, phase identification was carried out by electron beam diffraction under TEM. A select area diffraction (SAD) pattern inside the Ni_3P layer is shown in Fig. 6. Both Ni_3P and Ni are identified. A similar result was also obtained by other researchers.^{5,20} Based on the fact that the P

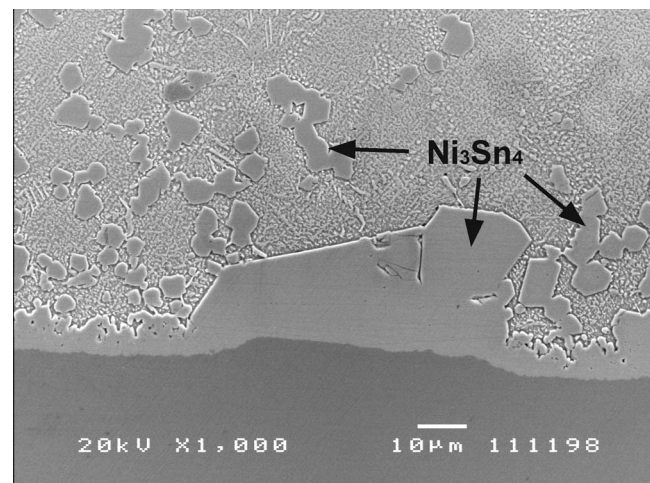


Fig. 4. Observation of IMC spallation but no delamination on 250- μm Ni foil. Samples reflowed at 251°C for 18 h.

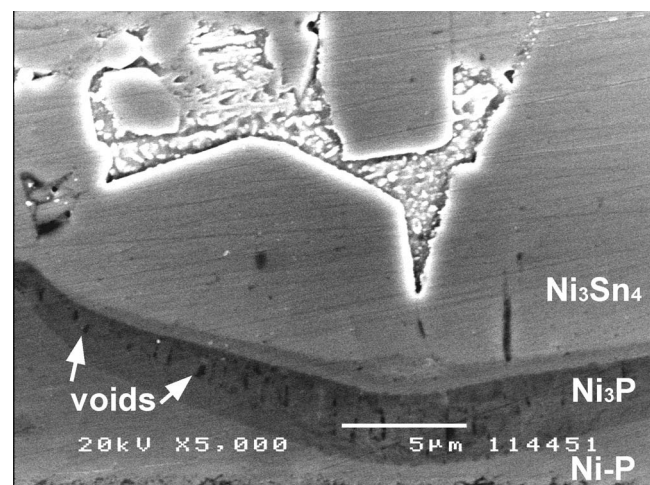


Fig. 5. Kirkendall voids formed in the Ni_3P layer in the Sn-3.5 Ag/Ni-P UBM system reflowed at 251°C for 1 h. The Ni-Sn-P layer is revealed between the Ni_3Sn_4 IMC and Ni_3P layers.

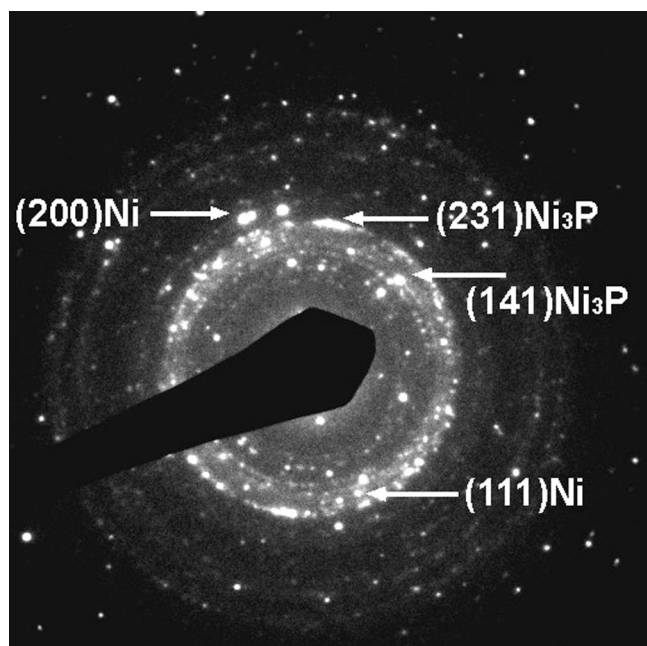
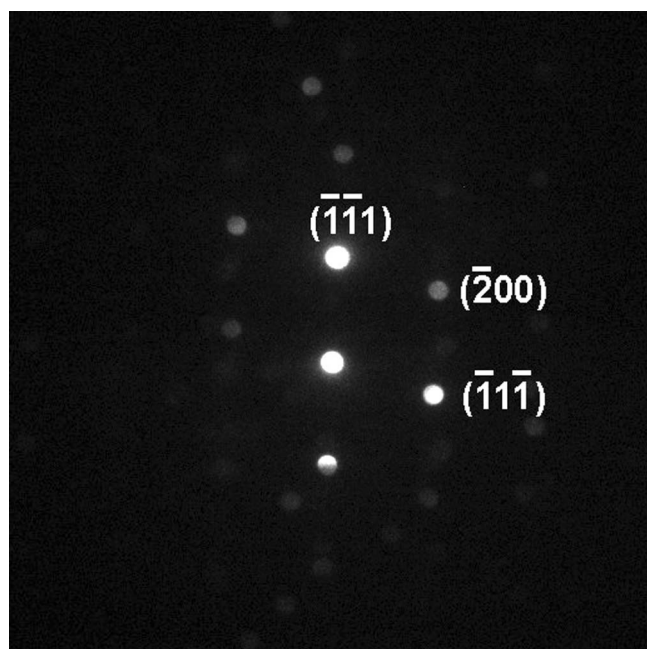


Fig. 6. The SAD patterns inside the Ni₃P layer. Both Ni₃P and Ni phases are identified.

concentration in this layer is close to the stoichiometric P content in Ni₃P, Ni₃P is the majority phase within the Ni₃P + Ni mixture. For convenience, this layer will still be addressed as the Ni₃P layer. In the Ni-Sn-P layer, EDX analysis showed that it does not have a fixed element composition.¹⁹ A nanobeam (15 nm in diameter) diffraction (NBD) pattern in Fig. 7 reveals the existence of both Ni₂SnP and Ni phases. Again for convenience, this layer is addressed as Ni-Sn-P.



a

Solid-State Solder: UBM Reaction

Ni₃Sn₄ IMC Growth during Solid-State Reaction

The thickness of the Ni₃Sn₄ layer is found to increase linearly with the square root of aging time and grows faster at higher temperatures. The results are shown in Fig. 8. The results indicate that the IMC growth in both systems is a diffusion-controlled process. The relationship between the IMC thickness and square root of time can be represented by

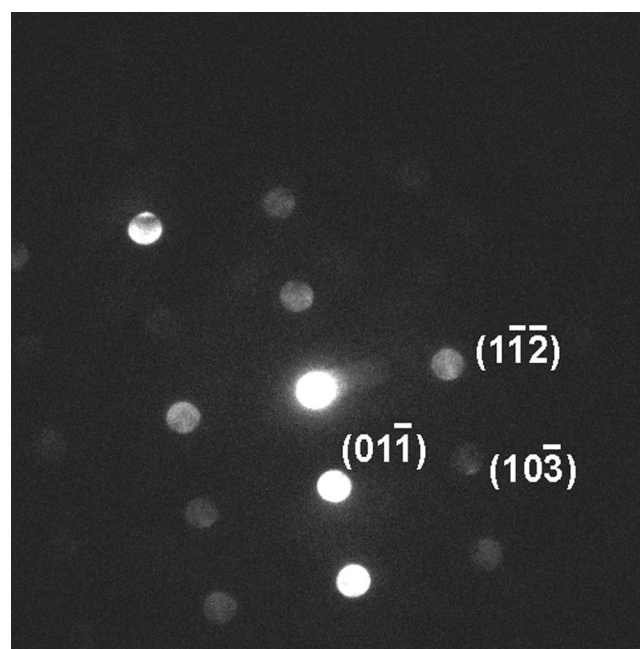
$$\delta = \delta_0 + k_s \sqrt{t} \quad (2)$$

where δ and δ_0 are the thickness of the IMC at time t and zero, respectively, and k_s is the solid-state growth rate constant. The k_s value, at a particular temperature, can be calculated by the slope of the linear fitting lines.

The diffusion coefficient, D , is represented by the Arrhenius equation:

$$D = k_s^2 A \exp(-Q/RT) \quad (3)$$

where A is a prefactor, T is the absolute temperature, R is the gas constant, and Q is the effective activation energy of the reaction. Table II summarizes the diffusivity values. An Arrhenius plot, as shown in Fig. 9, is obtained for the Sn-3.5Ag solder with the Ni-P and Ni UBMs. The activation energy for the Ni₃Sn₄ growth in a solid-state reaction is estimated to be 110 kJ/mol for the Sn-3.5Ag solder with the Ni-P UBM and 91 kJ/mol for the Sn-3.5Ag solder with the Ni UBM. The pre-exponential coefficients are 0.22 and 1.2×10^{-3} cm²/sec for the Ni-P and Ni UBMs, respectively. The smaller Q value associated with the Ni UBM system indicates IMC growth is



b

Fig. 7. The NBD patterns in the Ni-Sn-P layer: (a) Ni with a zone axis of $\langle 111 \rangle$ and (b) Ni₂SnP with a zone axis of $\langle 311 \rangle$.

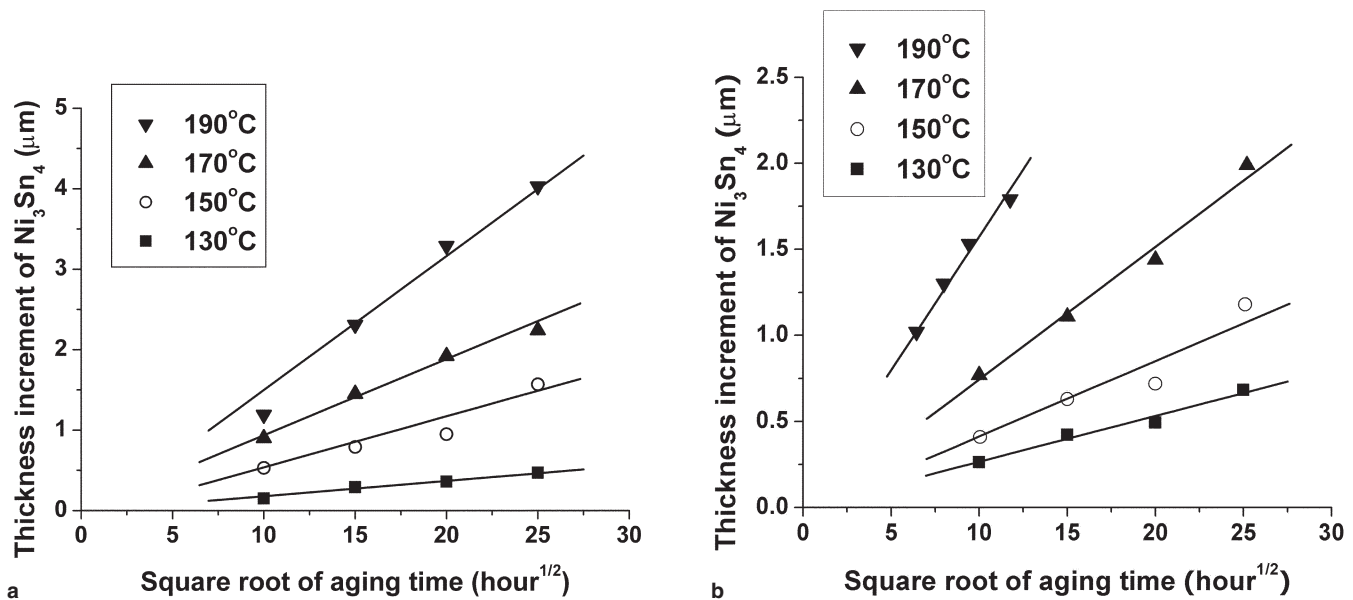


Fig. 8. Thickening kinetics of the Ni_3Sn_4 layer in Sn-3.5Ag/Ni-based UBM systems in solid-state reaction: (a) Ni-P UBM and (b) sputtered Ni UBM.

Table II. The diffusivity (cm^2/sec) for the Sn-3.5Ag Solder with Ni-P and Ni UBMs during Solid-State Reaction

Aging Temperature	130°C	150°C	170°C	190°C
Ni-P	9.99×10^{-16}	1.12×10^{-14}	2.49×10^{-14}	7.70×10^{-14}
Sputtered Ni	1.97×10^{-15}	5.34×10^{-15}	1.65×10^{-14}	6.73×10^{-14}

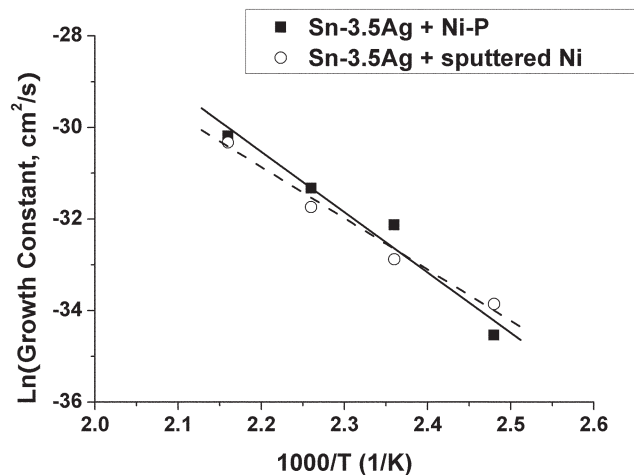


Fig. 9. Arrhenius plot for the formation of the Ni_3Sn_4 IMC between Sn-3.5Ag and Ni-based UBMs.

less sensitive to temperature in this system than the Ni-P system.

Kirkendall Void Growth during Aging

For the short reflow time before aging, Kirkendall voids are not observable under SEM. After prolonged heat treatment, they are seen inside the Ni_3P layer. The SEM-observable voids and their sizes depend on the thermal aging temperature and duration.¹⁹ No voids are observed under SEM in the samples aged at 130°C for as long as 625 h in the Sn-3.5Ag/Ni-P

samples. The voids can be found after a long period of aging at 150°C. For temperatures at 170°C and above, voids are detected after a relatively short aging time. The size and the number of visible voids increase with aging time.

DISCUSSION

IMC Spallation during Liquid-State Reaction

The IMCs spall into the molten solder for two reasons. The first is the mechanical stresses caused by the volume difference between the reaction metallization and the formed IMC. The other reason is delamination caused by poor wettability of the IMC to the underlying layer after the top UBM is fully consumed. During current work, we have verified that as long as Ni or Ni-P still exists, complete delamination will not occur. On the other hand, spalled IMCs are seen inside molten solder in spite of the good adhesion, and this spallation is more severe with the Ni UBM than Ni-P. The difference could be due to the nature of the stress generated at the interface. The density of the Ni-P alloy containing 12.5at.%P is around 8 g/cm^3 , while the densities of pure Ni and the Ni_3Sn_4 IMC are 8.9 g/cm^3 and 8.64 g/cm^3 , respectively. Although it is difficult to estimate the magnitude of the stress during the formation of IMC through this liquid-solid reaction, it is reasonable to suggest that the nature of stress is compressive when the IMC is formed on the pure Ni UBM. As the IMC layer becomes thick, the

compressive stress tends to squeeze out some IMCs, causing spallation. In the case of the Ni-P UBM, the stress is tensile in the IMC layer. A tensile stress, once built up sufficiently, may cause fracture of a continuous layer but not spallation. In fact, the IMC layer is not really continuous at the early stage of reflow because there are many grooves between neighboring grains. Therefore, the tensile stress may not be too serious a concern, especially at the initial stage of reflow.

Effect of P on IMC Formation and Growth

A notable difference between solder reactions with the two UBMs is the formation of the crystalline Ni_3P phase with Ni-P. The Ni_3P forms as a result of Ni depletion from the UBM to form Ni_3Sn_4 , which has facilitated the crystallization of the amorphous Ni-P.¹⁰ The Ni_3P layer consists of very fine grains. These fine grains affect the diffusion of Ni through this layer. Relatively faster diffusion of nickel at certain locations may result in different shapes and thicknesses of the Ni_3Sn_4 IMC grains along the interface. This could be the reason why the borderline becomes wavy in the Ni-P system. In the case of the Ni UBM, only the Ni_3Sn_4 IMC is formed by direct consumption of nickel. The consumption of Ni is uniform across the interface. As a result, the borderline is more straight.

The Ni-Sn-P layer is visible under SEM from samples aged at relatively high temperatures with long duration.¹⁹ It is also detectable in the sample reflowed for a long time (Fig. 5). Both the Ni_3P and Ni-Sn-P layers are formed because of the existence of P in the UBM.

During liquid-state reactions, the average thickness of the Ni_3Sn_4 IMC formed on the Ni-P UBM is found to be greater than the one on the Ni UBM for the same reflow process. During solid-state thermal aging, the IMC grows faster with the Ni-P UBM at higher temperatures (150°C and above). At lower aging temperatures, IMC growth rate is slower with the Ni-P UBM. Regardless of whether the solder is in a molten or solid state, the general trend is that at high reaction temperatures, the IMC growth in the Ni-P system is always faster than the Ni UBM, and this trend reverses at low temperatures. This gives rise to higher effective activation energy for the formation of Ni_3Sn_4 in the Ni-P system. We believe the formation of the ternary layer Ni-Sn-P plays an important role. From our experimental observation, at low reaction temperature, the Ni-Sn-P layer grows very slowly. Its growth could be the limiting factor for the overall diffusion process. At higher temperatures, however, the Ni-Sn-P layer grows much faster. It no longer serves as the “pace maker” for the overall interdiffusion between the solder and UBM. The difference in the growth kinetics of Ni_3Sn_4 in the two UBM systems may be influenced by different factors at different stages of reaction. What makes it different in the Ni-P system is the release of heat during formation of the Ni_3P

and Ni-Sn-P phases, as well as recrystallization of the amorphous Ni-P UBM. The additional energy release may promote the diffusion to speed up the IMC growth.

Kirkendall Void Formation

The formation of Kirkendall voids inside the Ni_3P layer is a phenomenon closely related with the Ni-P UBM. No such voids are observed with pure Ni UBM. This suggests that the presence of the Ni_3P layer and the Ni-Sn-P between the IMC and the UBM is a necessary condition for void formation. At the very beginning of the solder reaction, the formation of Ni_3Sn_4 depletes Ni from the surface of the electroless nickel alloy, resulting in crystallization of the P-enriched portion of the alloy to form Ni_3P .¹⁰ Further supply of nickel for the growth of Ni_3Sn_4 may come from two sources: decomposition of Ni_3P at the reaction front or the diffusion of nickel from the unreacted Ni-P through the Ni_3P layer. Detailed deliberation was carried out elsewhere by the current authors.¹⁹ What could be concluded is that for further growth of Ni_3Sn_4 , the provision of Ni must come from the unreacted Ni-P UBM layer. While Ni can diffuse through the Ni_3P layer easily, Sn is stopped because of the formation of an additional Ni-Sn-P layer.¹⁹ This causes a net out-flux of Ni both from the Ni-P UBM to the Ni_3P layer and from the Ni_3P layer to the Ni_3Sn_4 IMC. The unbalanced diffusion leads to the formation of the voids.

CONCLUSIONS

In this study, we compared the morphology and growth kinetics of the IMCs formed between Sn-3.5Ag and Ni-based UBMs (electroless Ni-P and sputtered Ni). Three distinctive layers, the Ni_3Sn_4 , Ni_3P , and Ni-Sn-P, form between the Sn-3.5Ag solder and Ni-P UBM as a result of the Sn/Ni-P reaction. In the case of the Ni UBM, only one layer of Ni_3Sn_4 is present between the solder and the UBM.

During liquid-state solder reaction, IMC thickness increases with reflow time following a power law with the power indices around 1/3 for both systems. The IMC growth rate is higher with the Ni-P UBM than the Ni UBM. Kirkendall voids are observed inside the Ni_3P layer in the Ni-P UBM system after long-time reflow. No voids are formed in the Ni UBM system.

Thermal aging resulted in growth of the intermetallics both in terms of overall thickness and crystal grain sizes. The thickness of the Ni_3Sn_4 layer increases linearly with the square root of thermal aging time in UBM systems, indicating that the formation of the IMCs is a diffusion-controlled process. The activation energy for Ni_3Sn_4 growth in solid-state reaction is found to be 110 kJ/mol and 91 kJ/mol for the Ni-P and sputtered Ni UBMs, respectively. Kirkendall voids are detected inside the Ni_3P layer in the Sn-3.5Ag/Ni-P system after long-term thermal aging.

In the process of IMC growth, Ni diffuses toward the direction of solder and Sn toward the direction of UBM. With the Ni UBM, the interfacial reaction only produces a layer of the Ni₃Sn₄ IMC; no Kirkendall voids have been observed. With the Ni-P UBM, the formation and growth of the Ni₃Sn₄ layer is similar to the one with the Ni UBM. In addition, the Ni₃P and Ni-Sn-P layers also form. The Ni diffuses through the two layers to react with Sn, while the counter flux of Sn stops at the interface between Ni₃Sn₄ and Ni₃P to form the Ni-Sn-P layer. This unbalanced interdiffusion leads to the formation of voids appearing inside the Ni₃P layer.

ACKNOWLEDGEMENTS

Financial support in the form of the Academic Research Fund from the Nanyang Technological University is gratefully acknowledged.

REFERENCES

1. K. Zeng and K.N. Tu, *Mater. Sci. Eng.* R38, 55–105 (2002).
2. K.N. Tu and K. Zeng, *Mater. Sci. Eng.* R34, 1–58 (2001).
3. A.A. Liu, H.K. Kim, and K.N. Tu, *J. Appl. Phys.* 80, 2774–2780 (1996).
4. H.K. Kim, K.N. Tu, and P.A. Totta, *Appl. Phys. Lett.* 68, 2204–2206 (1996).
5. P.L. Liu and J.K. Shang, *Metall. Mater. Trans. A* 31A, 2857–2866 (2000).
6. Y.C. Chan, P.L. Tu, C.W. Tang, K.C. Hung, and K.L. Lai, *IEEE Trans. Adv. Packaging* 24, 25–32 (2001).
7. K.L. Lin and Y.C. Liu, *IEEE Trans. Adv. Packaging* 22, 568–572 (1999).
8. L.C. Wang, Z. Mei, and R.H. Dauskardt, *MRS Symp. Proc.* (Warrendale, PA: MRS, 1999), pp. 3–8.
9. C.Y. Lee and K.L. Lin, *Thin Solid Films* 249, 201–206 (1994).
10. J.W. Jang, P.G. Kim, and K.N. Tu, *J. Appl. Phys.* 85, 8456–8463 (1999).
11. K.C. Hung, Y.C. Chan, C.W. Tang, and H.C. Ong, *J. Mater. Res.* 15, 2354–2539 (2000).
12. K.C. Hung and Y.C. Chan, *J. Mater. Sci. Lett.* 19, 1755–1757 (2000).
13. P.L. Liu and J.K. Shang, *J. Mater. Res.* 15, 2347–2355 (2000).
14. C.Y. Lee and K.L. Lin, *INTERPACK* 95, 26–30 (1995).
15. K. Kulojarvi, V. Vuorinen, and J. Kivilahti, *Microelectron. Int.* 15, 20–24 (1998).
16. J.W. Jang, D.R. Peter, T.Y. Lee, and K.N. Tu, *J. Appl. Phys.* 88, 6359–6363 (2000).
17. Y.D. Jeon, K.W. Paik, K.S. Bok, W.S. Choi, and C.L. Cho, *J. Electron. Mater.* 31, 520–528 (2002).
18. G. Qi, M. He, and Z. Chen, *Proc. Yazawa Int. Symp., in Conjunction with the 132nd TMS Annual Meeting Exhibition* (Warrendale, PA: TMS, 2003), pp. 1173–1184.
19. M. He, Z. Chen, and G. Qi, *Acta Mater.* 52, 2047–2056 (2004).
20. C.W. Hwang, K. Suganuma, M. Kiso, and S. Hashimoto, *J. Mater. Res.* 18, 2540–2543 (2003).
21. S.J. Wang and C.Y. Liu, *Scripta Mater.* 49, 813–818 (2003).
22. H. Matsuki, H. Ibuka, and H. Saka, *Sci. Technol. Adv. Mater.* 3, 261–270 (2002).
23. S. Ahat, M. Sheng, and L. Luo, *J. Mater. Res.* 16, 2914–2921 (2001).
24. M.O. Alam, Y.C. Chan, and K.C. Hung, *J. Electron. Mater.* 31, 1117–1121 (2002).
25. C.E. Ho, W.T. Chen, and C.R. Kao, *J. Electron. Mater.* 30, 379–385 (2001).
26. M. He, W.H. Lau, G. Qi, and Z. Chen, *Thin Solid Films*, 462–463, 376–383 (2004).